

Extension of Hartree–Fock theory including tensor correlation in nuclear matter

Jinniu Hu^{1,2,*,\dagger}, Hiroshi Toki^{1,*,\dagger}, and Yoko Ogawa^{1,*,\dagger}

¹Research Center for Nuclear Physics (RCNP), Osaka University, Ibaraki, Osaka 567-0047, Japan

²State Key Laboratory of Nuclear Physics and Technology, School of Physics, Peking University, Beijing 100871, China

*E-mail: jinnihu@rcnp.osaka-u.ac.jp (JH), toki@rcnp.osaka-u.ac.jp (HT), ogaway@rcnp.osaka-u.ac.jp (YO)

Received November 11, 2012; Revised March 25, 2013; Accepted August 11, 2013; Published October 1, 2013

.....
 We study the properties of nuclear matter in the extension of Hartree–Fock theory including tensor correlation using a realistic nucleon–nucleon (NN) interaction. The nuclear wave function consists of the Hartree–Fock and two-particle–two-hole ($2p-2h$) states, following the concept of the tensor-optimized shell model (TOSM) for light nuclei. The short range repulsion and strong tensor force of realistic NN interaction provide high momentum components, which are taken into account in a many-body framework by introducing $2p-2h$ states. Single particle states are determined by the variational principle of the total energy with respect to $2p-2h$ amplitudes and Hartree–Fock (HF) single-particle states. The resulting differential equation is almost identical with that of Brueckner–Hartree–Fock (BHF) theory by taking two-body scattering terms only. We calculate the equation of state (EOS) of nuclear matter in this framework with the Bonn potential as a realistic NN interaction. We found similar results to BHF theory with slightly repulsive effects in the total energy. The relativistic effect is discussed for the EOSs of nuclear matter in both non-relativistic and relativistic frameworks. The momentum distribution has large components at high momenta due to $2p-2h$ excitations. We also obtain the EOSs of pure neutron matter, where the tensor effect is small in the iso-vector channel.

Subject Index D04,D10,D11

1. Introduction

One central problem of nuclear physics is the description of the properties of finite nuclei and nuclear matter using the realistic nucleon–nucleon (NN) interaction, which is obtained from the phase shift data of NN scattering. Such a technique is usually called the microscopic many-body method, or *ab initio* method. A wide variety of microscopic methods were developed for light nuclei, whose masses are less than $A \sim 12$, and nuclear matter in the past 50 years. The variational method, as the most successful one, proposed by Jastrow [1], has evolved to the Green’s function Monte Carlo (GFMC) method, which was able to reproduce the ground and few excited states of light nuclei to masses up to $A \sim 12$ [2]. Furthermore, this variational method was also applied to the study of infinite nuclear matter [3]. Another famous microscopic method, Brueckner–Hartree–Fock (BHF) theory is derived from the Bethe–Goldstone equation of two-body scattering, whose solution is the G -matrix [4]. This G -matrix is an effective NN interaction including medium effects of surrounding nucleons. The BHF theory was mainly used successfully for the calculation of infinite nuclear matter [5].

^{\dagger}These authors contributed equally to this work.

The essential point in the microscopic many-body method is properly treating strong repulsive central force at short distance and strong tensor force, which are two important characters of realistic NN interaction. The short range repulsive interaction comes from the quark structure of the nucleon [6,7]. It can be dealt with using the Jastrow correlation function or unitary correlation operator method (UCOM) [8,9]. However, there are not so many powerful techniques for the treatment of the tensor force, since it has a wide interaction range. The role of the tensor force is clearly seen in the lightest nuclei, such as the deuteron. The tensor operator $S_{12}(\hat{r}) = \sqrt{24\pi/5}[Y_2(\hat{r}) \times [\sigma_1\sigma_2]^{(2)}]^{(0)}$ has the spherical harmonic function $Y_2(\hat{r})$ and the spin operator of rank two $[\sigma_1\sigma_2]^{(2)}$, and therefore acts simultaneously in the spatial and spin spaces. The transition matrix element from S - to D -states gives the largest attraction to bind a proton-neutron pair and at the same time introduces high momentum components in the wave function [10]. Usually, the D -wave probability is of the order of 5% for the deuteron. Meanwhile, the tensor force is also shown to provide strong shell effects as the spin-orbit splitting energy for heavy nuclear systems [11–15].

A drastic approximation in the description of light nuclei is introduced using the fact that the transition matrix element gives the largest contribution for the deuteron binding energy. This model, called the tensor-optimized few-body model (TOFM) [16], assumes that the wave function of a nucleus consists of only two states, $|\Psi\rangle = |\Psi_S\rangle + |\Psi_D\rangle$. The condition of the D -state is to have a non-zero matrix element of the tensor interaction with the S -state, $\langle\Psi_D|S_{12}(\hat{r})|\Psi_S\rangle \neq 0$. This choice of taking only one D -state was motivated by the success of the tensor-optimized shell model (TOSM) applied to ${}^4\text{He}$ by Myo et al. [17]. The results of TOFM are in very good agreement with those of the rigorous calculations for $A = 3, 4$ systems [18–20]. In addition, TOSM has been applied successfully to various phenomena such as halo formation and structures of the He and Li isotopes [21,22].

With this achievement in mind, a new many-body theoretical framework in the spirit of TOSM was developed based on the Hartree–Fock (HF) approximation to treat heavier nuclei ($A > 12$), where the shell structures appear in various observables. In this many-body theory, where the important role of the tensor interaction is taken into account, the ground state wave function is taken as a mixture of HF and two-particle–two-hole ($2p$ – $2h$) states, $|\Psi\rangle = C_0|0\rangle + \sum_{\alpha} C_{\alpha}|2p - 2h, \alpha\rangle$ [23]. Here, α distinguishes many $2p$ – $2h$ states. The coefficients of $2p$ – $2h$ states and single particle states are obtained by the variational principle of the total energy for the whole system. With this extension, the tensor force can be explicitly included in the Hartree–Fock framework.

The tensor effect is small in pure neutron matter for the isospin triplet $T = 1$ channel [24]. However, the tensor force plays a very important role in the saturation mechanism of symmetric nuclear matter and contributes very largely at the second-order perturbation level [25,26]. Furthermore, the symmetry energy of infinite nuclear matter is also shown as mainly provided by the tensor force due to the isospin dependence in the framework of the BHF theory with a realistic NN interaction, AV18 potential [27]. It is very interesting to calculate how many high momentum components are involved for the strong tensor and short range repulsive correlations.

Hence, the motivation of this work is to study the properties of nuclear matter in the extended HF theory including tensor correlation using a realistic NN interaction beyond the perturbation treatment on tensor force. We would like to discuss the properties of EOSs by explicitly treating high momentum components. We show the momentum distributions in infinite nuclear matter. We will discuss the properties of nuclear matter in this theory for different isospin cases and the high momentum behaviors of nucleons due to $2p$ – $2h$ components. In Sect. 2, we derive the extension of HF theory including tensor correlation (HFT) following the TOSM so that it can be applied to nuclear matter systems. In Sect. 3, numerical results are presented for the properties of nuclear matter. We study

both symmetric and pure neutron matter in relativistic and non-relativistic frameworks. We present momentum distributions and the numbers of high momentum components due to short range and tensor correlations. In Sect. 4, we will give a summary of the present work.

2. The extension of HF theory including tensor correlation

The HF theory, an approximation of a many-body quantum system, is very popular for use in the study of finite nuclei and infinite nuclear matter, and has been widely used over the years [28,29]. However, there is a serious problem in this approximation if it is seen from a microscopic view point. This problem is related to the fact that the expectation value of the tensor force is zero in the HF state of spin-saturated systems. Hence, we are not able to study the role of the pion, which produces a strong tensor force, in finite nuclei and nuclear matter. To overcome this problem, we introduce $2p-2h$ excited states in the ground state wave function, following the TOSM for light nuclei proposed by Myo et al. [17]. The $2p-2h$ states can treat the tensor force explicitly and include high momentum components.

We write the Hamiltonian of nuclear matter, where the realistic NN interaction is written in the one-boson-exchange form as the Bonn potential,

$$H = \int d^3\mathbf{x} \bar{\psi}(\mathbf{x}) (-i\boldsymbol{\gamma} \cdot \nabla + M_N) \psi(\mathbf{x}) + \frac{1}{2} \sum_{\substack{i=\sigma,\delta, \\ \eta,\pi,\omega,\rho}} \int d^3\mathbf{x}' d^3\mathbf{x} \bar{\psi}(\mathbf{x}') \bar{\psi}(\mathbf{x}) \Gamma_i(1, 2) G_i(\mathbf{x} - \mathbf{x}') \psi(\mathbf{x}') \psi(\mathbf{x}), \quad (1)$$

where $G_i(\mathbf{x} - \mathbf{x}')$ are the propagators of various mesons exchanged between two nucleons,

$$G_i(\mathbf{x} - \mathbf{x}') = \frac{1}{4\pi} \frac{e^{-m_i|\mathbf{x}-\mathbf{x}'|}}{|\mathbf{x} - \mathbf{x}'|}. \quad (2)$$

The one-boson-exchange potential is defined as a sum of one-particle amplitudes of six bosons, with π and η pseudoscalar, σ and δ scalar, and ρ and ω vector mesons.

The various Γ_i represent Dirac matrices and coupling constants between nucleon and meson vertices which are listed below:

$$\begin{aligned} \Gamma_\sigma(1, 2) &= -g_\sigma^2, \\ \Gamma_\delta(1, 2) &= -g_\delta^2 \boldsymbol{\tau}_1 \cdot \boldsymbol{\tau}_2, \\ \Gamma_\eta(1, 2) &= -\left(\frac{f_\eta}{m_\eta}\right)^2 (/q\gamma_5)_1 (/q\gamma_5)_2, \\ \Gamma_\pi(1, 2) &= -\left(\frac{f_\pi}{m_\pi}\right)^2 (/q\gamma_5)_1 (/q\gamma_5)_2 \boldsymbol{\tau}_1 \cdot \boldsymbol{\tau}_2, \\ \Gamma_\omega(1, 2) &= g_\omega^2 \gamma_\mu(1) \gamma^\mu(2), \\ \Gamma_\rho^V(1, 2) &= g_\rho^2 \gamma_\mu(1) \gamma^\mu(2) \boldsymbol{\tau}_1 \cdot \boldsymbol{\tau}_2, \\ \Gamma_\rho^T(1, 2) &= \left(\frac{f_\rho}{2M_N}\right)^2 q_\nu \sigma^{\mu\nu}(1) q^\lambda \sigma_{\mu\lambda}(2) \boldsymbol{\tau}_1 \cdot \boldsymbol{\tau}_2, \\ \Gamma_\rho^{VT}(1, 2) &= i \left(\frac{g_\rho f_\rho}{M_N}\right) \gamma_\mu(2) \sigma^{\mu\nu} q_\nu(1) \boldsymbol{\tau}_1 \cdot \boldsymbol{\tau}_2. \end{aligned} \quad (3)$$

Here, $\sigma_{\mu\nu} = \frac{i}{2}[\gamma_\mu, \gamma_\nu]$ is the antisymmetric tensor operator of gamma matrices, and the tensor coupling part between ω meson and nucleon has been neglected for the value of f_ω/g_ω is very small.

We include the form factor for all the meson exchange interactions with the parameters of the Bonn potential.

In the Hamiltonian, the field operator $\psi(\mathbf{x})$ can be expanded by a creation operator c_i^\dagger and an annihilation operator c_i of i state. Therefore, this Hamiltonian in a second quantization form is:

$$H = T + V$$

$$= \sum_{\alpha\beta} \langle \alpha | T | \beta \rangle c_\alpha^\dagger c_\beta + \frac{1}{2} \sum_{\alpha\beta\gamma\delta} \langle \alpha\beta | V | \gamma\delta \rangle c_\alpha^\dagger c_\beta^\dagger c_\delta c_\gamma, \quad (4)$$

where the indices, α, \dots , include quantum numbers of momentum, spin, and isospin in all possible states. It can be split into particle and hole states to express more clearly using particle and hole operators a_i and b_i ,

$$c_i = \theta(i - F)a_i + \theta(F - i)b_i^\dagger. \quad (5)$$

Here, F represents the Fermi state and the θ function is the step function defined by

$$\theta(F - i) = \begin{cases} 1, & \text{if } i \leq F, \\ 0, & \text{if } i > F. \end{cases} \quad (6)$$

The tilde state \tilde{i} represents a time reversal state of i .

We assume that the ground state wave function is composed of HF and $2p-2h$ states,

$$|\Psi\rangle = C_0|0\rangle + \sum_{\alpha} C_{\alpha}|\alpha\rangle. \quad (7)$$

Here, $|0\rangle$ is the HF ground state and α represents the quantum numbers of $2p-2h$ states,

$$\alpha = \{i, j, k, l\} \begin{cases} i, j < F, \\ k, l > F. \end{cases} \quad (8)$$

Here, i, j denote hole states and k, l particle states. Furthermore, we should keep in mind that these indices represent not only the momentum of corresponding states, but also the spin and isospin. This wave function is expressed by particle and hole operators,

$$|\Psi\rangle = C_0|0\rangle + \sum_{\alpha} C_{\alpha} a_k^\dagger a_l^\dagger b_i^\dagger b_j^\dagger |0\rangle. \quad (9)$$

Here, all the $2p-2h$ states are ordered and therefore they are orthonormalized. For the coefficients C_0 and C_{α} , they fulfill the normalization condition,

$$|C_0|^2 + \sum_{\alpha} |C_{\alpha}|^2 = 1. \quad (10)$$

Using the Hamiltonian and the ground state wave function, the total energy of the whole system can be written as,

$$\begin{aligned} \langle \Psi | H | \Psi \rangle &= |C_0|^2 \langle 0 | H | 0 \rangle + \sum_{\alpha} C_0^* C_{\alpha} \langle 0 | H | \alpha \rangle \\ &+ \sum_{\beta} C_{\beta}^* C_0 \langle \beta | H | 0 \rangle + \sum_{\alpha, \beta} C_{\beta}^* C_{\alpha} \langle \beta | H | \alpha \rangle. \end{aligned} \quad (11)$$

The first term of the right-hand side is generated by the HF state. The other three terms arise from the contribution of $2p-2h$ states. The strong tensor and short range correlation effects are contained in

these terms. In finite nuclei, it was demonstrated that the tensor correlation can be treated by taking a reasonable number of $2p-2h$ states, while short range correlation needs too many $2p-2h$ states and is treated by the unitary correlation method [17]. In infinite matter, we are able to express even the short range correlation in this framework due to the fact that $2p-2h$ states are represented in plane wave states.

It is obvious that there are many matrix elements in the total energy, which should be calculated one by one. The first one is the matrix element of the HF state,

$$\langle 0|H|0\rangle = \sum_{i<F} \langle i|T|i\rangle + \frac{1}{2} \sum_{i,j<F} \langle ij|V|ij\rangle_A. \quad (12)$$

This matrix element corresponds to the standard HF energy. The next one is matrix elements between HF and $2p-2h$ states,

$$\langle 0|H|\alpha\rangle = \langle ij|V|kl\rangle - \langle ij|V|lk\rangle = \langle ij|V|kl\rangle_A, \quad (13)$$

where the subscript A means the antisymmetrization. Here, the kinetic energy as a one-body operator does not provide any contribution in this matrix element.

The final one corresponds to matrix elements among $2p-2h$ states. These matrix elements are very complicated and include the HF energy,

$$\langle \beta|H|\alpha\rangle = \langle 0|H|0\rangle\delta_{\alpha,\beta} + \langle \beta|\tilde{H}|\alpha\rangle, \quad (14)$$

where $\langle \beta|\tilde{H}|\alpha\rangle$ are matrix elements of the Hamiltonian, which are related explicitly with $2p-2h$ states. The explicit expressions of these matrix elements are written in Ref. [23].

There are two kinds of variational quantities in the total energy, which are coefficients in the ground state wave function C_α and single particle wave functions $\psi_i(\mathbf{x})$. We want to determine them through the variational principle of the total energy,

$$\begin{aligned} \frac{\delta[\langle \Psi|H|\Psi\rangle - E(C_0^*C_0 + \sum_\alpha C_\alpha^*C_\alpha)]}{\delta C_\alpha^*} &= 0, \\ \frac{\delta[\langle \Psi|H|\Psi\rangle - \sum_i \varepsilon_i \int d^3\mathbf{x} \psi_i^*(\mathbf{x})\psi_i(\mathbf{x})]}{\delta \psi_i^*(\mathbf{x})} &= 0. \end{aligned} \quad (15)$$

The total energy E and the single particle energy ε_i are the Lagrange multipliers in the variational method.

These two variational equations can be expressed explicitly as,

$$C_0 \langle \alpha|H|0\rangle + \sum_\beta C_\beta \langle \alpha|H|\beta\rangle = EC_\alpha, \quad (16)$$

and

$$\begin{aligned} T|i\rangle + \sum_j \langle \cdot j|V|ij\rangle_A + C_0^* \sum_\alpha C_\alpha \frac{\partial}{\partial \psi_i^*(\mathbf{x})} \langle 0|H|\alpha\rangle \\ + \sum_{\alpha,\beta} C_\beta^* C_\alpha \frac{\partial}{\partial \psi_i^*(\mathbf{x})} \langle \beta|\tilde{H}|\alpha\rangle = \varepsilon_i|i\rangle. \end{aligned} \quad (17)$$

In the equation of motion of single-particle states, the first two terms correspond to the ordinary HF terms. The last two pieces come from contributions of $2p-2h$ states. After we solve these two equations concerning coefficients and single-particle states exactly, the total energy E of the whole

system can be obtained. The above modified HF equation motivates us to introduce an effective Hamiltonian to be used for the HF state,

$$H_{\text{eff}} = |C_0|^2 \left(H - \sum_{\alpha, \beta} V|\alpha\rangle\langle\alpha| \frac{1}{H - E} |\beta\rangle\langle\beta| V \right). \quad (18)$$

With this effective Hamiltonian, we obtain the differential equations for single particle states in the extended HF theory by taking the variation of the HF matrix element of H_{eff} [23],

$$\langle 0|H_{\text{eff}}|0\rangle = |C_0|^2 \langle 0|T + V|0\rangle - |C_0|^2 \sum_{\alpha, \beta} \langle 0|V|\alpha\rangle\langle\alpha| \frac{1}{H - E} |\beta\rangle\langle\beta|V|0\rangle. \quad (19)$$

The resulting differential equation agrees with the extended HF equation (17) in which C_α are eliminated by using the relation for the amplitudes (16).

Here, the operator in the denominator has the following matrix elements,

$$\langle\alpha|H - E|\beta\rangle = (\langle 0|H|0\rangle - E)\delta_{\alpha\beta} + \langle\alpha|\tilde{H}|\beta\rangle, \quad (20)$$

where E in this equation is the ground state energy. It is important to note that the HF energy $\langle 0|H|0\rangle$ and the total energy appear in the matrix elements in Eq. (20). Here we take the HF approximation to calculate particle-particle matrix elements.

$$\begin{aligned} \langle\alpha|\tilde{H}|\beta\rangle &= \langle\alpha|T + V|\beta\rangle \\ &\sim \langle\alpha|\tilde{H}_{\text{HF}} + (V - U)|\beta\rangle, \end{aligned} \quad (21)$$

where U is the HF single-particle potential. This U is obtained by the HF procedure, where the modified HF interaction \tilde{G} is calculated by including the $\langle 0|H|0\rangle - E$ term in the denominator as shown in Eq. (22). We approximate to take only particle-particle matrix elements of the residual interaction $V - U$ by using the bare interaction V , where the two-body interaction V connects many $2p$ states as compared with the one-body operator U .

We have an extended HF theory including tensor correlation. We denote this framework as HFT. In the HFT theory, we first calculate the effective HF interaction \tilde{G} .

$$\begin{aligned} \langle ij|\tilde{G}|ij\rangle &= \langle ij|V|ij\rangle - \sum_{\substack{\alpha(ij p_1 p_2) \\ \beta(ij p'_1 p'_2)}} \langle 0|V|\alpha\rangle\langle\alpha| \frac{1}{\langle 0|H|0\rangle - E + \tilde{H}_{\text{HF}} + V} |\beta\rangle\langle\beta|V|0\rangle \\ &= \langle ij|V|ij\rangle - \sum_{\substack{\alpha(ij p_1 p_2) \\ \beta(ij p'_1 p'_2)}} \langle 0|V|\alpha\rangle\langle\alpha| \frac{1}{\langle 0|H|0\rangle - E + \tilde{H}_{\text{HF}}} |\beta\rangle\langle\beta|\tilde{G}|0\rangle. \end{aligned} \quad (22)$$

After getting the effective HF interaction using above equation in the standard method, we solve a modified HF equation as

$$|C_0|^2 \left(T + \sum_j \frac{\partial}{\partial \psi_i^*(\mathbf{x})} \langle ij|\tilde{G}|ij\rangle_A \right) \psi_i(\mathbf{x}) = \varepsilon_i \psi_i(\mathbf{x}). \quad (23)$$

We note that the $|C_0|^2$ appearing here is removed by the variation of the denominator having $\langle 0|H|0\rangle$ as shown in Eq. (17), where the normalization condition $|C_0|^2 + \sum_\alpha |C_\alpha|^2 = 1$ is used. We can find that the structure of effective HF interaction, \tilde{G} , is very similar to the G -matrix in the BHF theory.

From here on, we follow the method of the RBHF theory of Brockmann and Machleidt [5]. The equation of motion of single particle states in a relativistic framework for nuclear matter should follow the Dirac equation,

$$(\boldsymbol{\alpha} \cdot \mathbf{p}_i + \beta M_N + \beta U)u(\mathbf{p}_i, s_i) = \varepsilon_i u(\mathbf{p}_i, s_i), \quad (24)$$

where $\psi_i(\mathbf{x}) = \sum_{p_i, s_i} u(\mathbf{p}_i, s_i) e^{-i\mathbf{x} \cdot \mathbf{p}_i}$, and the single-particle potential U is composed of scalar potential U_S and vector potential U_V ,

$$U = U_S + \gamma^0 U_V, \quad (25)$$

and $u(\mathbf{p}_i, s_i)$ is the Dirac spinor

$$u(\mathbf{p}_i, s_i) = \left(\frac{M_N^* + E_i^*}{2M_N^*} \right)^{1/2} \begin{bmatrix} 1 \\ \boldsymbol{\sigma} \cdot \mathbf{p}_i \\ M_N^* + E_i^* \end{bmatrix} \chi(s_i). \quad (26)$$

Here, M_N^* is the effective nucleon mass and E_i^* the effective nucleon energy, defined respectively as

$$\begin{aligned} M_N^* &= M_N + U_S, \\ E_i^* &= \sqrt{M_N^{*2} + \mathbf{p}_i^2}, \end{aligned} \quad (27)$$

where χ_s is the Pauli spinor corresponding to spin states.

With this Dirac equation, we can obtain the single-particle energy ε_i as

$$\begin{aligned} \varepsilon_i &= \frac{M_N^* M_N + p_i^2}{E_i^*} + \sum_{j < F} \frac{M_N^{*2}}{E_i^* E_j^*} |C_0|^2 \langle ij | \tilde{G} | ij \rangle_A \\ &= E_i^* + U_V, \end{aligned} \quad (28)$$

where in order to obtain the second line of this equation we have used an identity about the single particle potential,

$$U(i) = \frac{M_N^*}{E_i^*} \langle i | U_S + \gamma^0 U_V | i \rangle = \frac{M_N^*}{E_i^*} U_S + U_V. \quad (29)$$

Thus, in the actual numerical calculation, we first assume an initial effective nucleon mass M_N^* and vector potential U_V . We can take them to solve the extended HF equation, Eq. (22), and obtain the \tilde{G} -matrix. With this initial \tilde{G} -matrix, we generate a new effective nucleon mass M_N^* and vector potential U_V . Then, the initial single-particle energy ε_i at the different momentum can be calculated through the first line of Eq. (28). The new effective nucleon mass M_N^* and vector potential U_V can be extracted from the second line of Eq. (28). Following this procedure, we can get the exact effective nucleon mass and vector potential until the iteration results become stable. With exact single-particle states and coefficients, we can get the total energy E of the whole system. All these procedures are worked out in the relativistic Hartree–Fock theory including tensor correlation (RHFT).

If M_N^* is replaced by M_N in Eq. (28), we speak of the non-relativistic Hartree–Fock theory including tensor correlation (HFT), since in this case the spinor structure is fixed at the free case and the resulting equations correspond to the non-relativistic Brueckner–Hartree–Fock theory [5]. In such a

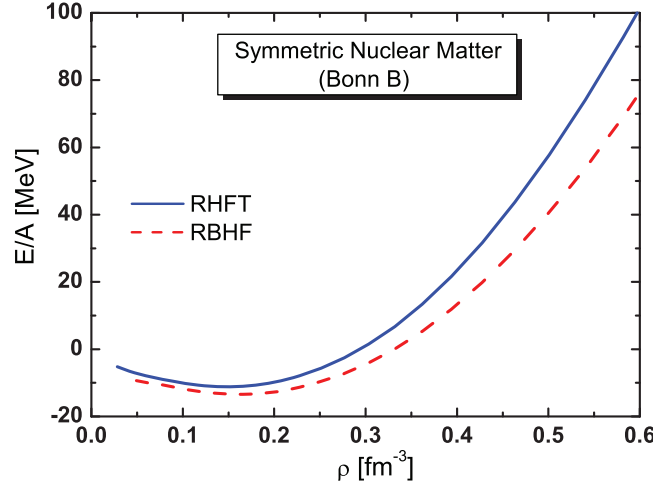


Fig. 1. The EOS of symmetric nuclear matter using the Bonn-B potential in the RHFT and RBHF theories as a function of nuclear matter density. The solid curve is the EOS in the RHFT theory, while the dashed one is the result of the RBHF theory [5].

case, the single particle energy becomes

$$\begin{aligned} \varepsilon_i &= E_i + \sum_{j < F} \frac{M_N^2}{E_i E_j} |C_0|^2 \langle ij | \tilde{G} | ij \rangle_A \\ &= \sqrt{M_N^{*2} + p_i^2} - M_N^* + M_N + U_0, \end{aligned} \quad (30)$$

where the single-particle energy is parameterized by an effective nucleon mass M_N^* and a single-particle potential U_0 . The relativistic effect is extremely important for the behavior of the equation of state in the high density region.

3. Numerical results

In this section, we provide numerical results using the Bonn potentials as realistic NN interactions to study the properties of nuclear matter in HFT. There are three kinds of Bonn potentials, Bonn-A, Bonn-B, and Bonn-C [30]. They were generated by fitting the phase shifts of NN scattering. The largest difference among them appears in the strength of the tensor force. This quantity is reflected in the D -state probability of the deuteron, P_D . Bonn-A potential has the weakest tensor component with $P_D = 4.5\%$. Bonn-B and Bonn-C provide $P_D = 5.1\%$ and $P_D = 5.5\%$, respectively. When we solve Eq. (22), the angle-average approximation on the Pauli operator is adopted and the contribution of partial waves is included until $J < 9$.

We show first the EOS of symmetric nuclear matter with the Bonn-B potential in Fig. 1 in RHFT theory. The binding energy per particle is shown as a function of density. We give the results of the relativistic BHF (RBHF) theory [5] with the same potential in this figure as a dashed curve for comparison. The binding energy is $E/A = -11.48$ MeV at the saturation density $\rho_0 = 0.1484$ fm $^{-3}$ in the RHFT theory. The saturation density becomes smaller compared with the saturation density $\rho_0 = 0.1625$ fm $^{-3}$ in the RBHF theory, while the system is bound less than the one in the RBHF theory, where $E/A = -13.44$ MeV. We find that the total energies in RHFT are higher than the ones in RBHF in the whole density region. This additional repulsive contribution in RHFT comes from the coefficient of the HF ground state $|C_0|^2$ and the modified HF $2p$ - $2h$ energy $\tilde{E}_{2p-2h} = E_{2p-2h} + \langle 0|H|0 \rangle - E$. The HF probability $|C_0|^2$ reduces the magnitude of the G -matrix. \tilde{E}_{2p-2h}

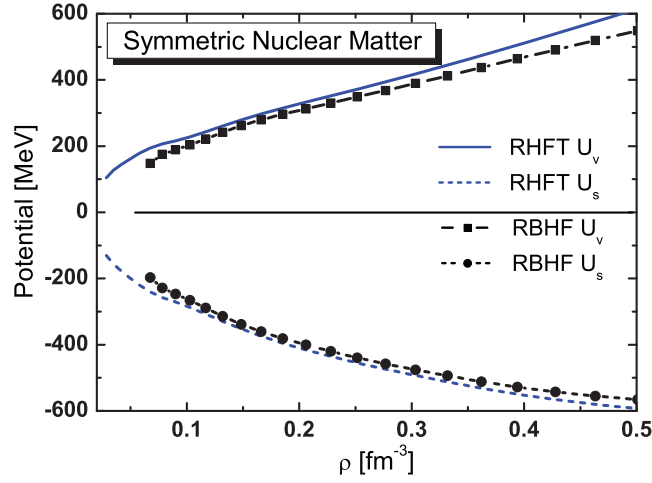


Fig. 2. The scalar (negative side) and vector potentials (positive side) in symmetric nuclear matter with Bonn-B potential in the RHFT and RBHF theories [5].

can also influence the G -matrix when we solve the effective HF equation. The modified $2p-2h$ energy contains not only the single-particle energy, but also the HF energy and total energy.

The key point of our numerical calculation is to get the scalar potential U_S and vector potential U_V in Eq. (25) following the method of Brockmann and Machleidt [5], which parameterizes the single-particle energy ε_i and effective nucleon mass M_N^* . These two components of the single-particle potential for symmetric nuclear matter as a function of density are plotted in Fig. 2 with the Bonn-B potential in RHFT. The vector potential provides a repulsive effect, while the scalar potential gives an attractive effect. Their summation is about -60 MeV at the saturation density. These potentials can reproduce spin-orbit splittings for finite nuclei. This can be regarded as the theoretical foundation of the relativistic mean field theory, which is a very successful and effective theory in the many-body problem. We also compare these two potentials with the results obtained in the RBHF theory. At low density, they are very similar. The difference between the two theories becomes larger as the density increases. The variation of the vector potential U_V is more visible. The more repulsive contribution directly causes the decrease of the binding energy.

The nucleon mass is not constant in a many-body system, which is influenced by other nucleons around it. The medium effect, which becomes larger as the density increases, can be represented by the effective nucleon mass M_N^* . In the relativistic framework, we can define the effective nucleon mass as $M_N^* = M_N + U_S$, which is also called the Dirac mass. This effective nucleon mass M_N^* is shown in Fig. 3 as a function of density in the RHFT theory. It is about $0.62M_N$ at the saturation density, which is consistent with the empirical data on nuclear matter around $0.60M_N \sim 0.70M_N$ at the saturation density. This effective nucleon mass in the RHFT theory is very similar to that in the RBHF theory, since their scalar potentials are similar.

The momentum distribution $n(k)$ is an important quantity to show high momentum components due to short range and tensor correlations. In the HF theory, the momentum distribution is described by the step function,

$$n(k) = \begin{cases} 1 & k < k_F, \\ 0 & k > k_F. \end{cases}$$

This implies that all the single-particle states in the HF state stay under the Fermi surface. There is no probability in particle states, although the short range and tensor correlations induce high momentum

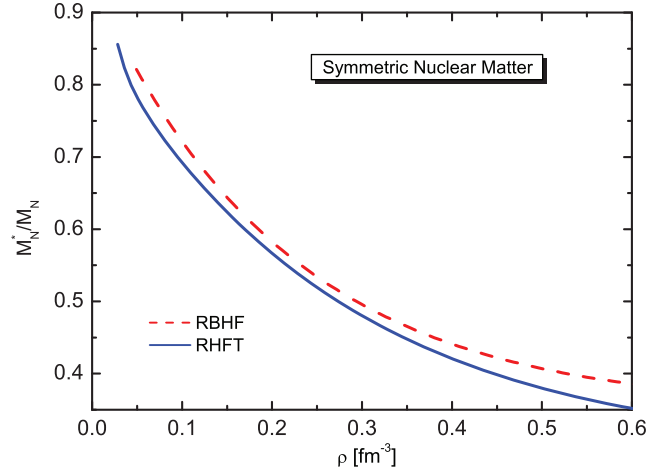


Fig. 3. The effective nucleon mass in symmetric nuclear matter with Bonn-B potential in the RHFT and RBHF theories. The solid curve corresponds the results of RHFT, while the dashed curve is for RBHF [5].

components. In the BHF theory, Baldo et al. made a further calculation including the mass operator to study the momentum distribution using the G -matrix and obtained some probabilities above the Fermi momentum [31]. Now, after introducing $2p-2h$ excited states in the ground state wave function, there is some probability of momenta higher than the Fermi momentum due to the $2p-2h$ states. The momentum distribution is no longer the step function, even at the extended Hartree–Fock level. Now we can define the momentum distribution of hole states $n(i)$ as,

$$\begin{aligned} n(i) &= \langle \Psi | b_i b_i^\dagger | \Psi \rangle \\ &= 1 - \sum_{jkl} 2C_\alpha^* C_\alpha, \end{aligned} \quad (31)$$

and momentum distribution of particle states $n(k)$,

$$\begin{aligned} n(k) &= \langle \Psi | a_k^\dagger a_k | \Psi \rangle \\ &= \sum_{ijl} 2C_\alpha^* C_\alpha, \end{aligned} \quad (32)$$

where the subscripts of coefficient α represent different i, j, k, l and $i, j < k_F, k, l > k_F$. Furthermore, the momentum distribution should also satisfy the identity

$$4 \int \frac{d^3 \mathbf{k}}{(2\pi)^3} n(k) = \rho_B. \quad (33)$$

Therefore we get the normalization

$$\int \frac{dk}{k_F} 3 \left(\frac{k}{k_F} \right)^2 n(k) = 1. \quad (34)$$

With this definition of the momentum distribution, we show the momentum distribution of particle and hole states in the RHFT theory with the Bonn-B potential at $k_F = 1.30 \text{ fm}^{-1}$ in panel (a) of Fig. 4. We find that the momentum distribution of hole states reduces to about 0.8 at the Fermi surface. The occupation probability above the Fermi momentum is about 0.2 close to Fermi momentum, $k_F = 1.3 \text{ fm}^{-1}$, due to the presence of the $2p-2h$ states. This conclusion is consistent with the result of the self-consistent Green's function method of Dickhoff et al. [32]. We also give the normalized

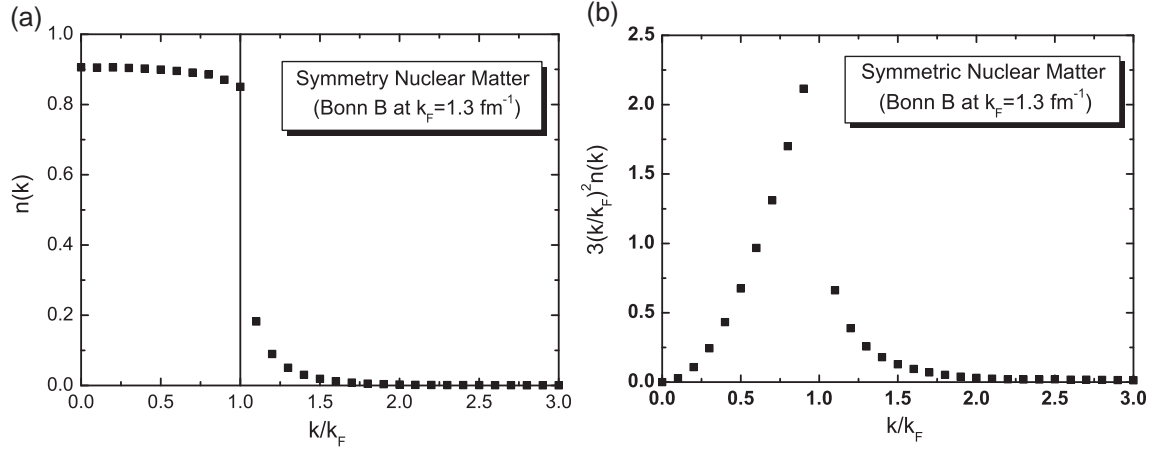


Fig. 4. (a) The momentum distribution at the saturation density with the Fermi momentum $k_F = 1.30 \text{ fm}^{-1}$ for symmetric nuclear matter in the RHFT theory with the Bonn-B potential. (b) The momentum distribution is multiplied by a factor to ensure its integral is normalized to one.

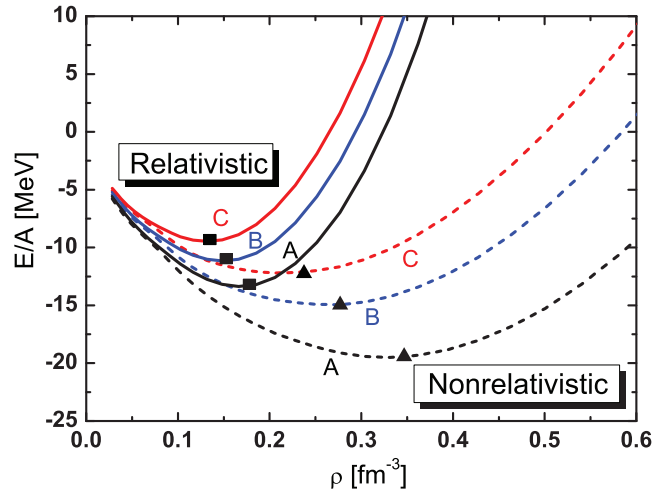


Fig. 5. The EOSs of symmetric nuclear matter with the Bonn-A, Bonn-B, and Bonn-C potentials in the RHFT and HFT theories as functions of nuclear matter density ρ . The solid curves represent the relativistic case, while the dashed curves the non-relativistic case. The symbols (solid square points and solid triangle points) represent the saturation points, respectively.

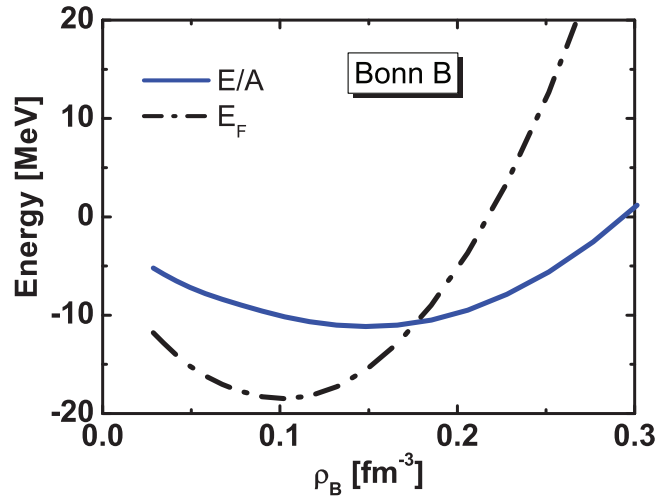
momentum distribution (34) in panel (b) by multiplying the momentum distribution by some factor. It is normalized to one to reflect the momentum distribution sum-rule.

We study EOSs of symmetric nuclear matter using other Bonn potentials, Bonn-A, Bonn-B, and Bonn-C, in the HFT and RHFT theories and show the results in Fig. 5. In the RHFT theory (solid curves), the EOS of the Bonn-A potential has the largest binding energy, while the Bonn-C has the smallest one. This difference increases with the nuclear matter density. Their saturation densities and binding energies form the “Coester line,” where the strength of the tensor force determines the location of the nuclear matter saturation point.

The saturation properties of symmetric nuclear matter in the RHFT and RBHF theories with the three Bonn potentials have been listed in Table 1. The binding energy of each potential at the saturation density in the RHFT theory is smaller than that of the RBHF theory, while the saturation densities are smaller than those of the RBHF theory. The incompressibilities of symmetric nuclear

Table 1. The saturation properties of symmetric nuclear matter in the RHFT theory and RBHF theory [5] with Bonn potentials.

Methods	Potential	ρ [fm^{-3}]	E/A [MeV]	K [MeV]	M_N^*/M_N	$ C_0 ^2$
RBHF	Bonn A	0.1814	-15.38	302.9	0.598	1.0
	Bonn B	0.1625	-13.44	240.3	0.621	1.0
	Bonn C	0.1484	-12.12	181.6	0.640	1.0
RHFT	Bonn A	0.1699	-13.62	272.7	0.601	0.911
	Bonn B	0.1484	-11.48	210.5	0.625	0.905
	Bonn C	0.1320	-9.80	163.9	0.648	0.901

**Fig. 6.** The energy per particle E/A (solid curve) and the Fermi energy E_F (dashed curve) are shown as functions of density for the case of Bonn-B potential in the RHFT theory in relation to the HvH theorem [33].

matter in the RHFT theory are reduced to a smaller value than the RBHF result due to a smaller saturation density. This means that the EOSs in RHFT are softer than those of RBHF. The binding energies at the saturation density in the RHFT theory are smaller than the empirical value, around $E/A = -16 \pm 1$ MeV. A few MeV of attractive contribution is missing in our theory, which may be provided by the Fujita–Miyazawa-type three-body interaction [2]. Furthermore, we would like to discuss our results in terms of Hugenholtz–van Hove (HvH) theorem, $E/A + P/\rho = E_F$ [33]. To this end, we show in Fig. 6 the energy per particle E/A and the Fermi energy E_F as a function of density for the case of Bonn-B potential in the RHFT theory. The energy per particle E/A and the Fermi energy E_F seem to approximately fulfill the HvH theorem, but the crossing point of the two curves slightly deviates from the saturation point, where the pressure P is zero. This slight breaking of the HvH theorem might be caused by an approximation used for the extraction of the scalar and vector potentials in Eq. (25) following the method of RBHF theory by Brockmann and Machleidt [5]. This point should be clarified in the near future.

In the non-relativistic HFT theory (dashed curves), the effective nucleon mass M_N^* in the Dirac spinor is replaced by the free nucleon mass M_N . The saturation energy is $E/A = -14.94$ MeV at the saturation density $\rho_0 = 0.2767 \text{ fm}^{-3}$. This saturation density is very far from the empirical data, which is around $\rho_0 = 0.16 \text{ fm}^{-3}$. The relativistic effect is seen in the difference between the

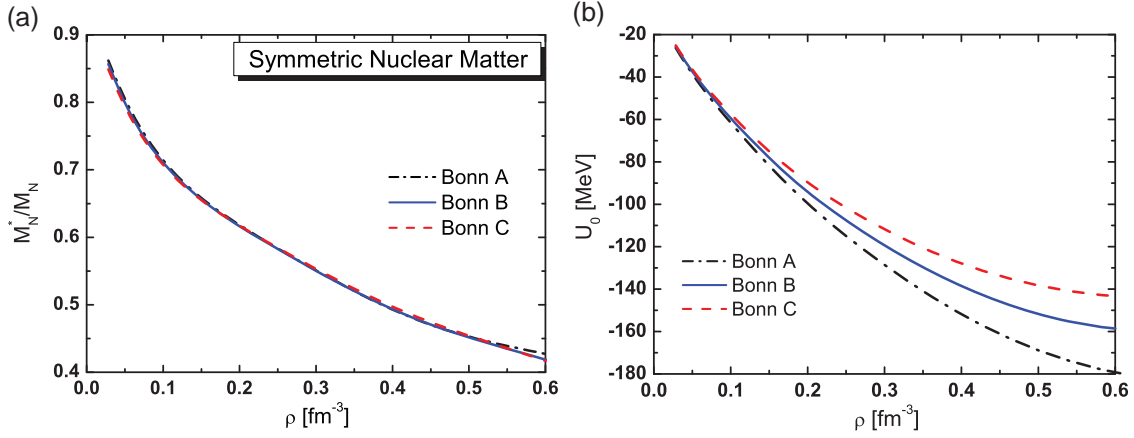


Fig. 7. The effective masses and single-particle potentials of symmetric nuclear matter with different Bonn potentials in the HFT theory. In panel (a), the effective nucleon masses are given, while the single-particle potentials are shown in panel (b). In both panels, the dot-dashed line is the result for the Bonn-A potential, solid for the Bonn-B potential, and dashed for the Bonn-C potential.

RHFT and HFT theories, which is highly repulsive. This repulsive effect makes the saturation density improve significantly, while the binding energy becomes smaller. Furthermore, a comparison between relativistic and nonrelativistic HFT calculations for all three Bonn potentials is given in Fig. 5. The Coester line in the nonrelativistic approach is shifted toward lower saturation density for the new Coester line of the relativistic approach. The binding energies are different from the empirical one by about 3.0 MeV in the relativistic case. The relativistic framework contains the repulsive three-body force through the Z -graph mechanism [34]. In the RBHF theory, we do not have any clue of the attractive three-body effect. In RHFT theory, we have the room to introduce the three-body force of Fujita–Miyazawa type through the Δ isobar excitation [35]. In fact, in the variational method worked out by Akmal et al. [3] with three-body force, Urbana IX, the three-body force provided about 4 MeV attraction at the saturation density. If we can obtain a similar contribution from the three-body attractive force, the EOS in RHFT theory will be in agreement with the empirical value.

We show in Fig. 7 the effective nucleon mass M_N^* and single-particle potential $U_0 = U_S + U_V$. The effective nucleon masses for the three potentials are almost identical in the whole density region. The single-particle potentials are very similar below 0.15 fm^{-3} . As the density increases, the single-particle potential for Bonn-A obtains more attractive effect, which makes the binding energy of Bonn-A the largest among the three potentials.

The EOSs of pure neutron matter with Bonn-A, Bonn-B, and Bonn-C potentials in RHFT theory are plotted in Fig. 8 and compared with that in RBHF theory. Their EOSs are almost identical in the whole density region. This result is the same as in the RBHF theory [36]. The study of pure neutron matter is very important for the application to astrophysics [37], such as neutron stars and supernova explosion. Pure neutron matter is not self-bound and their total energy is positive. We find there is a repulsive effect in the EOS of RHFT in comparison with RBHF [5]. The results in RHFT agree with those of the RHFJ model [38], where the Jastrow function is introduced in the wave function part to take short range correlation into account. The magnitude of the Jastrow function is determined by the variational principle on the total energy. We have explained that the difference of these three potentials is in the tensor components. However, the tensor effect is very weak in pure neutron matter for the isospin $T = 1$ channel.

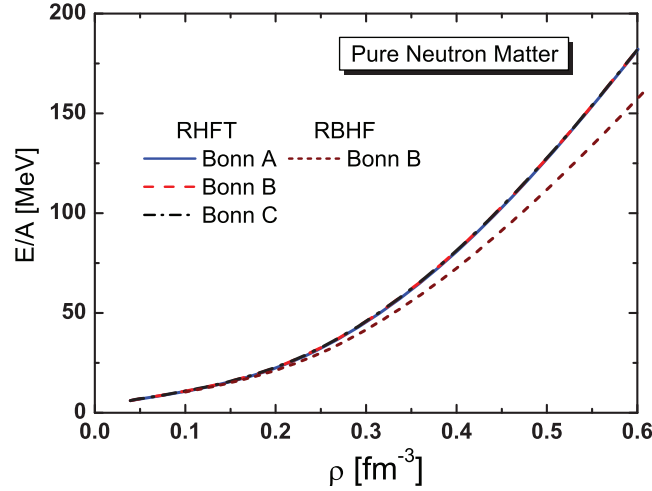


Fig. 8. The EOSs of pure neutron matter with Bonn-A, Bonn-B, and Bonn-C potentials in RHFT theory. The solid curve represents EOSs of Bonn-A, dashed curve for Bonn-B, and dot-dashed for Bonn-C. The dotted curve denotes the EOS calculated in RBHF using the Bonn-B potential.

Finally, we study the Hartree–Fock and $2p-2h$ components in the ground state wave function. The quantity $|C_0|^2$ is denoted as the probability of the Hartree–Fock state and the rest, $\sum_{\alpha} |C_{\alpha}|^2 = 1 - |C_0|^2$, corresponds to the number of $2p-2h$ states. We give $|C_0|^2$ of symmetric nuclear matter and pure neutron matter in RHFT theory for the three Bonn potentials in panel (a) of Fig. 9. The Hartree–Fock ground states occupy a significant amount in the nuclear wave function since $|C_0|^2$ is above 80% in the whole density, which means that the $2p-2h$ states only provide about 20% contribution in the total wave function. However, this 20% takes the short range correlation and tensor correlation caused by the realistic NN interaction and provides the saturation mechanism of symmetric nuclear matter. Furthermore, we also notice that the tensor correlation is largest in the low density region. The probability $|C_0|^2$ increases at low density in symmetric nuclear matter. This behavior demonstrates that the effect of $2p-2h$ correlation is gradually reduced with increasing density. On the other hand, in pure neutron matter, this phenomenon does not exist. In this way, the tensor force provides the saturation mechanism of symmetric nuclear matter. When the density increases further, the short range correlation starts to be more important, since the distance between nucleons becomes shorter. The magnitude of $|C_0|^2$ in symmetric nuclear matter is different than that in pure neutron matter. In symmetric nuclear matter, the $2p-2h$ states are caused not only by the short range correlation but also by the tensor force, while they are caused only by the short range correlation in pure neutron matter. Therefore, the components of the $2p-2h$ states in symmetric nuclear matter are larger than the ones in pure neutron matter.

In panel (b) of Fig. 9, we compare the difference of the HF state for Bonn-B potential in symmetric nuclear matter (SNM) and pure neutron matter (PNM). This difference reduces with the density increase. This means that the effect of the tensor force taken by the $2p-2h$ states is reduced at higher densities, which can be represented by the difference in the probabilities of $0p-0h$ states between SNM and PNM. This tensor correlation effect is denoted by a solid curve in panel (b) of Fig. 9. At high density the tensor correlation tends to saturate. The short range correlation effect can be expressed as $1 - |C_0|^2$ in PNM, which is the amplitude of the $2p-2h$ states. The short range correlation increases with increasing density.

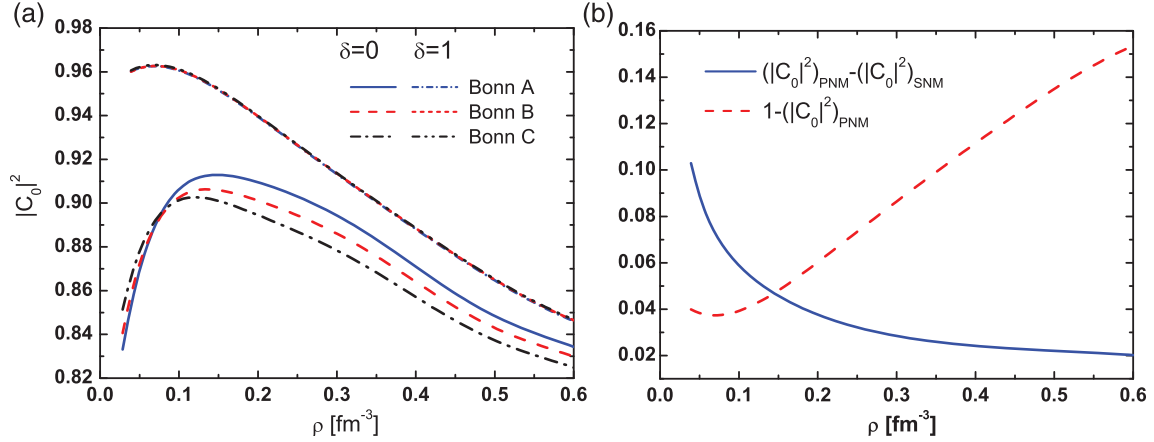


Fig. 9. In panel (a), $|C_0|^2$ of symmetric nuclear matter ($\delta = 0$) and pure neutron matter $\delta = 1$ in the RHFT theory for three Bonn potentials are provided. In panel (b), the tensor and short range correlations from $2p-2h$ states are shown for the case of Bonn-B potential. The solid curve corresponds to the tensor correlation and the dashed curve to short range correlation.

4. Summary and Conclusion

We have extended the Hartree–Fock theory including tensor correlation (HFT) by introducing $2p-2h$ states in the ground state wave function besides the Hartree–Fock ground state following the work of the tensor optimized shell model (TOSM). The short range correlation and strong tensor force of realistic NN interaction were taken into account by the $2p-2h$ excitation properly for the study of nuclear matter. We determined the components of the $2p-2h$ states in the nuclear wave function and single-particle state through the variational principle on the total energy of the whole system. The equation of motion of single-particle states obtained by the variational principle was composed of two parts. The first part was the traditional Hartree–Fock equation and the second part was generated by the $2p-2h$ component. From this equation of motion, we can obtain an effective NN interaction which includes $2p-2h$ correlations. When we limit the off-diagonal matrix elements of the $2p-2h$ states to particle-particle interactions, this effective NN interaction was closely related to the G -matrix in the BHF theory.

The properties of symmetric nuclear matter were studied with realistic NN interactions, the Bonn potentials, by the extension of HF theory including tensor correlation in the relativistic framework (RHFT). The binding energy of symmetric nuclear matter in the RHFT theory became smaller than the one in the RBHF theory. With this additional repulsive contribution, the saturation properties of symmetric nuclear matter in the RHFT theory become slightly above the empirical data. We also discussed the Hugenholtz–van Hove (HvH) theorem in RHFT theory. We found that it was almost fulfilled in RHFT theory, where a slight deviation might be caused by an approximation used for the extraction of scalar and vector potentials in the modified HF equations. The relativistic effect in the HFT theory provides strong repulsive effect, which can be interpreted as nucleon-antinucleon excitation (Z-graph) leading to repulsive three-body interaction. This conclusion reminds us that the attractive effect of three-body force should also be important in the RHFT theory. Furthermore, we found that this attractive component of three-body force could be included in the HFT theory with off-diagonal matrix elements between particle-hole channels. There are enough reasons for us to believe that the saturation properties of nuclear matter will be largely improved after we take the full calculation in the HFT theory including the delta isobars explicitly.

With the $2p-2h$ states, we also calculated the momentum distribution in the RHFT theory. The probability of particle state is about 20% at the Fermi surface, while it is impossible to have high momentum components above the Fermi momentum in the Hartree–Fock theory. The probability of hole state is about 80% close to the Fermi surface. These results were consistent with the results in the Green’s function method of Dickhoff et al. [32].

We also applied the RHFT theory to pure neutron matter. The EOS of pure neutron matter in RHFT theory is in agreement with the one in the RHFJ method [38], where the short range correlation was treated explicitly with the Jastrow function. The EOSs of Bonn-A, -B, and -C potentials in RHFT theory were almost identical, since the difference between these three potentials exists in the tensor components. However, the tensor effect is very weak in pure neutron matter for the isospin $T = 1$ channel. There was only the short range correlation for pure neutron matter in the RHFT theory. The amount of the Hartree–Fock state $|C_0|^2$ in the nuclear wave function was also shown. From this probability of the Hartree–Fock state, we found that the $2p-2h$ states took the tensor force mainly below the saturation density, while $2p-2h$ states were used for the short range correlation at high density. The components of $2p-2h$ states in symmetric nuclear matter were larger than in pure neutron matter since $2p-2h$ states were used for both the short range and tensor correlations in symmetric nuclear matter.

The success of the HFT theory for the description of nuclear matter encourages us to extend this framework to other aspects of nuclear physics, such as hyperon nuclear matter and finite nuclear systems. Of course, how to get the attractive effect from the three-body force to improve the saturation properties of nuclear matter is also a very interesting topic to be worked out in the future.

Acknowledgements

The authors are grateful to the members of the theory group of RCNP for clarifying the treatment of the pion in nuclear physics. This work is supported by the JSPS research grant 21540267. J. Hu is supported by the MEXT fellowship.

References

- [1] R. Jastrow, Phys. Rev. **98**, 1479 (1955).
- [2] S. C. Pieper and R. B. Wiringa, Annu. Rev. Nucl. Part. Sci. **51**, 53 (2001).
- [3] A. Akmal, V. R. Pandharipande, and D. G. Ravenhall, Phys. Rev. C **58**, 1804 (1998).
- [4] K. Brueckner, C. Levinson, and H. Mahmoud, Phys. Rev. **95**, 217 (1954).
- [5] R. Brockmann and R. Machleidt, Phys. Rev. C **42**, 1965 (1990).
- [6] H. Toki, Z. Physik A **294**, 173 (1980).
- [7] M. Oka and K. Yazaki, Prog. Theor. Phys. **66**, 556 (1981).
- [8] H. Feldmeier, T. Neff, R. Roth, and J. Schnack, Nucl. Phys. A **632**, 61 (1998).
- [9] T. Neff and H. Feldmeier, Nucl. Phys. A **713**, 311 (2003).
- [10] K. Ikeda, T. Myo, K. Kato, and H. Toki, Lecture Note in Phys. **818**, 165 (2010).
- [11] H. Toki, S. Sugimoto, and K. Ikeda, Prog. Theor. Phys. **108**, 903 (2002).
- [12] Y. Ogawa, H. Toki, S. Tamenaga, H. Shen, A. Hosaka, S. Sugimoto, and K. Ikeda, Prog. Theor. Phys. **111**, 75 (2004).
- [13] Y. Ogawa, H. Toki, and S. Tamenaga, Phys. Rev. C **76**, 014305 (2007).
- [14] S. Sugimoto, H. Toki, and K. Ikeda, Phys. Rev. C **76**, 054310 (2007).
- [15] Y. Ogawa and H. Toki, Nucl. Phys. A **860**, 22 (2011).
- [16] K. Horii, H. Toki, T. Myo, and K. Ikeda, Prog. Theor. Phys. **127**, 1019 (2012).
- [17] T. Myo, H. Toki, and K. Ikeda, Prog. Theor. Phys. **121**, 511 (2009).
- [18] H. Kamada et al., Phys. Rev. C **64**, 044001 (2001).
- [19] Y. Suzuki, W. Horiuchi, M. Orabi, and K. Arai, Few-Body Syst. **42**, 33 (2008).
- [20] E. Hiyama, Y. Kino, and M. Kamimura, Prog. Part. Nucl. Phys. **51**, 223 (2003).

- [21] T. Myo, A. Umeya, H. Toki, and K. Ikeda, Phys. Rev. C **84** 034315 (2011).
- [22] T. Myo, A. Umeya, H. Toki, and K. Ikeda, Phys. Rev. C **86** 024318 (2012).
- [23] Y. Ogawa and H. Toki, Ann. Phys. (N.Y.) **326**, 2039 (2011).
- [24] J. Hu, H. Toki, W. Wen, and H. Shen, Phys. Lett. B **687**, 271 (2010).
- [25] N. Kaiser and W. Weise, Nucl. Phys. A **697**, 255 (2002).
- [26] Y. Wang, J. Hu, H. Toki, and H. Shen, Prog. Theor. Phys. **127**, 739 (2012).
- [27] I. Vidaña, A. Polls, and C. Providência, Phys. Rev. C **84**, 062801(R) (2011).
- [28] D. Vautherin and D. M. Brink, Phys. Rev. C **5**, 626 (1972).
- [29] Y. Sugahara and H. Toki, Nucl. Phys. A **579**, 557 (1994).
- [30] R. Machleidt, Adv. Nul. Phys. **19**, 189 (1989).
- [31] M. Baldo, I. Bombaci, G. Giansiracusa, and U. Lombardo, Phys. Rev. C **41**, 1748 (1990).
- [32] W. H. Dickhoff and C. Barbieri, Prog. Part. Nucl. Phys. **52**, 377 (2004).
- [33] N. M. Hugenholtz and L. van Hove, Physica **14**, 363 (1958).
- [34] Z. H. Li, U. Lombardo, H.-J. Schulze, W. Zuo, L. W. Chen, and H. R. Ma, Phys. Rev. C **74**, 047304 (2006).
- [35] J. Fujita and H. Miyazawa, Prog. Theor. Phys. **17**, 360 (1957).
- [36] P. G. Krastev and F. Sammarruca, Phys. Rev. C **74**, 025808 (2006).
- [37] H. Shen, H. Toki, K. Oyamatsu, and K. Sumiyoshi, Nucl. Phys. A **637**, 435 (1998).
- [38] J. Hu, H. Toki, and H. Shen, J. Phys. G **38**, 085105 (2011).